PISCES

Plumes and Ices Simulation chamber for Enceladus and other moonS

Bourgeois, Yaël R.A.; Cazaux, Stéphanie M.

DOI
10.1016/j.pss.2025.106206

Publication date
2025

Document Version
Final published version

Published in
Planetary and Space Science

Planetary and Space Science 269 (2025) 106206

Contents lists available at ScienceDirect

Planetary and Space Science

journal homepage: www.elsevier.com/locate/pss

PISCES: Plumes and Ices Simulation chamber for Enceladus and other moonS

Yaël R.A. Bourgeois *, Stéphanie M. Cazaux

Faculty of Aerospace Engineering, Delft University of Technology, Delft, The Netherlands
Leiden Observatory, Leiden University, P.O. Box 9513, NL 2300 RA Leiden, The Netherlands

ARTICLE INFO

Keywords:
Enceladus
Plumes
Experiments
Vacuum chamber
Instrumentation

ABSTRACT

The discovery of vast subsurface oceans beneath the thick ice crusts of icy moons in our Solar System has ignited global interest in their potential habitability and in the processes shaping these celestial bodies. With upcoming missions set to explore the Galilean and Cronian moons in the coming decades, experimental studies are essential for optimising mission planning, selecting and testing scientific instruments, and maximising the scientific return from future observations. In this paper, we present the Plumes and Ices Simulation Chamber for Enceladus and other moonS (PISCES) — a novel experimental setup designed to replicate the extreme environmental conditions of icy moons, with pressures reaching down to 3×10^{-5} mbar and temperatures as low as 80 K. PISCES enables controlled laboratory investigations of plume dynamics and surface interactions using a suite of integrated sensors and instruments. We describe the vacuum chamber setup, its capabilities, and its adaptability to various experimental configurations. To demonstrate its potential, we detail experiments simulating Enceladus' plume activity with the Crevasse Laboratory Analogues for Moons (CLAM), an experimental apparatus employing 3D-printed cylindrical channels positioned above a liquid water reservoir within the vacuum chamber. This approach allows us to examine plume behaviour — including vent velocity, temperature, and particle size — in relation to subsurface conditions such as wall temperature, conduit dimensions, and expansion ratios. Ultimately, PISCES provides a groundbreaking platform for experimentally reproducing icy plumes under conditions analogous to those on Enceladus, advancing our understanding of plume physics and informing future planetary exploration efforts.

1. Introduction

Several objects in our Solar System are known (Nimmo and Pappalardo, 2016) —such as Enceladus (Iess et al., 2014), Europa (Khurana et al., 1998), Ganymede (Vance et al., 2014) —or strongly suspected, like Callisto (Khurana et al., 1998) and Mimas (Lainey et al., 2024), to harbour liquid water beneath an ice shell. Table 1 presents a non-exhaustive list of the primary bodies of interest for analogue studies, along with the temperature and pressure at the surface of the bodies, including Enceladus (Brown et al., 2006), Europa (Brown and Hand, 2013; Ligier et al., 2016), Ganymede (Ligier et al., 2019), and Triton (Cruikshank et al., 1993; Quirico et al., 1999; Lellouch et al., 2010). Space missions to study these unique worlds using remote sensing instruments and even *in situ* lander measurements would yield an invaluable wealth of data concerning habitability of such icy worlds.

With the discovery of plumes of water vapour and ice particles from Enceladus' south polar region in 2005 from the Cassini spacecraft (Porco et al., 2006), Enceladus has become the focal point of both NASA,[1] and ESA (Choblet et al., 2022) for future missions. Numerous studies have sought to characterise these plumes originating from elongated crevasses known as the "Tiger Stripes". The prevailing theory for plume formation involves the vaporisation of liquid water (Porco et al., 2006; Schmidt et al., 2008; Postberg et al., 2009) from a subsurface ocean beneath the ice shell inferred from gravity and libration measurements (Iess et al., 2014; Thomas et al., 2016). Cassini observations have provided key insights into plume characteristics, including vent temperatures (Spencer et al., 2006; Spencer and Nimmo, 2013), ice–vapour mass ratios and mass flow of particles (Gao et al., 2016; Kieffer et al., 2009; Ingersoll and Ewald, 2011), and supersonic plume velocities, determined with UVIS (Hansen et al., 2006, 2008, 2011; Tian et al., 2007; Portyankina et al., 2022) or INMS observations (Dong et al., 2011; Perry et al., 2015). Various theoretical models have been proposed to constrain the heat and mass transfer associated with Enceladus' geological activity observed by the Cassini mission (Matson et al., 2012; Kite and Rubin, 2016; Yeoh et al., 2015, 2017; Mitchell et al., 2024), as well as the geometry of the crevasses

* Corresponding author at: Faculty of Aerospace Engineering, Delft University of Technology, Delft, The Netherlands.
E-mail address: y.bourgeois@tudelft.nl (Y.R.A. Bourgeois).

[1] https://ntrs.nasa.gov/citations/20205008712 accessed March 31, 2025

https://doi.org/10.1016/j.pss.2025.106206
Received 7 May 2025; Received in revised form 1 September 2025; Accepted 9 October 2025
Available online 30 October 2025

Table 1
Surface properties of icy moons of interest and PISCES capabilities.

Name of body	Surface pressure	Surface temperature	Surface composition (%wt)
Enceladus	~1 mbar (*estimated at plume vent)	80 K (average) up to ~210 K	H_2O: 99%; CO_2: traces; NH_3: <2%
Europa	~1×10^{-9} mbar	90 K	Water ice - frozen mixed brines; $MgSO_4$: <47%; Na_2SO_4: <44%
Ganymede	0.2 to 1.2×10^{-8} mbar	100 K	H_2O & CO_2 ice; H_2SO_4 hydrates & salts: <10%
Triton	1.4×10^{-7} mbar to $4\sim6 \times 10^{-7}$ mbar	~38 K	N_2 ice - some CH_4 and CO; H_2O & CO_2: <45%; CH_4: <10%
PISCES	Chamber pressure: 3×10^{-5} to 1000 mbar	~80 to 300 K	User defined and controlled

Table 2
Enceladian plumes' physical characteristics.

Ice crust thickness	Vent temperature	Ice/Vapour mass ratio	Grain size	Plume velocity
~7 to 40 km	up to ~210 K	0.07 to 0.7	up to ~tens of μm	300 to 2000 m/s

and the conditions governing water vapour flow (Ingersoll and Pankine, 2010; Tucker et al., 2015; Nakajima and Ingersoll, 2016; Ingersoll and Nakajima, 2016; van der Hijden et al., 2024). Table 2 summarises the major known constraints from the preceding literature of the observed plumes of Enceladus.

Given the extensive timelines, complexity, and vast costs associated with space missions, there is a pressing need to prepare for and support the outcome of such missions by studying these celestial bodies in controlled environments.

The design and development of the Plumes and Ices Simulation Chamber for Enceladus and other moonS (PISCES) setup provides an experimental platform, enabling the emulation of both physical and chemical processes occurring in the interiors and on the surfaces of these icy worlds.

Environmental chambers such as PISCES have become increasingly popular for the experimental study of extra-terrestrial bodies, including Mars (Mars Environmental Simulation Chamber -MESCH- (Jensen et al., 2008), MARTE (Sobrado et al., 2014)), Venus (Glenn Extreme Environment Rig -GEER- (Chi et al., 2024), Venus Simulation Laboratory (Steenstra, 2024)), and more general planetary environments (Planetary Atmosphere and Surfaces Chamber -PASC- (Mateo-Marti, 2014), Planetary Analogues Laboratory for Light, Atmosphere, and Surface Simulation -PALLAS- (ten Kate and Reuver, 2016)). In the case of icy moons, small-scale experimental setups have been employed in the literature to investigate specific aspects, such as the optical properties and composition of deposited surface ice (Muñoz Caro et al., 2002; Bründl et al., 2022), the optical spectra of ice particles obtained from aerosolization of liquid water (Fox-Powell et al., 2022) or the chemistry of the rock/water interface in the enceladian core (Postberg, 2014; Sekine et al., 2015; Hamp et al., 2024).

However, no existing facility is designed to explore moon-scale processes, such as plume dynamics, under controlled laboratory conditions the way PISCES was built, with a detailed description of this setup provided in the following sections of this paper. Special attention has been given to the design of PISCES to allow support of focused investigations on the plumes' dynamics.

This setup is a key component of the Delft Planetary Laboratories, a synergistic research platform located at the Faculty of Aerospace Engineering at Delft University of Technology. It enables experiments under a wide range of planetary conditions, from the high-pressure, high-temperature environments of planetary interiors with the Venus Simulation Laboratory (Steenstra, 2024) to the low-pressure, low-temperature extremes characteristic of icy moons with PISCES and ICEBEAR (Kipfer et al., 2024).

This paper presents the current state of the PISCES experimental setup (Section 2.1), focusing on pressure, temperature, and associated measurement strategies (Section 2.2) in the context of plume dynamics investigations (Section 3.1) and planned survey of opto-mechanical properties of surface ices (Section 4)

2. PISCES

The PISCES setup is designed to study the wide range of conditions that occur in and on icy worlds. The final row of Table 1 details the range of conditions achievable within PISCES, described in the following section, illustrating the setup's capacity to replicate most of the physical and chemical environments encountered on icy bodies. It is not only suitable to emulate environmental conditions at their surface with various exospheric pressures and temperatures, but it can also be used to study replica of dynamic phenomena, most notably icy plumes, as observed on Enceladus.

2.1. The chamber

The chamber is an 800 × 800 × 800 mm inner dimension stainless steel cube designed and assembled by Vacuum Specials,[2] with a tested leak rate below 1.10^{-7} mbar.L/s and fitted with an extensive set of portholes and feedthroughs, as can be seen in Fig. 1.

The primary pumps are dual air-cooled ECODRY plus 40 (Leybold), a roots pump capable of reaching below 5.10^{-2} mbar ultimate partial pressure at a 40 m^3/h maximum pumping speed. They are connected in parallel, and the gas ballast feature allows a maximum water vapour outgassing rate of 300 g/h, as specified in the technical data. The second stage is a TURBOVAC 850 i(X) (Leybold) turbo-molecular pump, further reducing the ultimate pressure in the chamber down to 3.10^{-5} mbar. Fig. 2 shows the evolution of the absolute pressure inside PISCES under different pumping scenarii.

The chamber features an LN_2-cooled cold finger, serving a dual purpose. It is designed to collect condensed vapours and icy particles onto a witness plate for *in situ* optical analysis. It can also be used solely to reduce the pressure inside PISCES (as seen with the black curve in Fig. 2), by acting as a cold trap, condensing some of the matter that the pumps cannot remove from the chamber.

Finally, PISCES is equipped with four 180 mm diameter portholes at the centre of each sidewall (including the door) and a larger 230 mm diameter porthole on the top. Two sets of window materials are available: borosilicate glass and sapphire glass, depending on experimental requirements.

2.1.1. Feedthroughs

The right side of the chamber features eleven DN40 KF flanges to interface with various sensors and instruments (see Fig. 3). Among these, the following are installed:

[2] http://www.vacuumspecials.nl/en/ accessed April 2, 2025

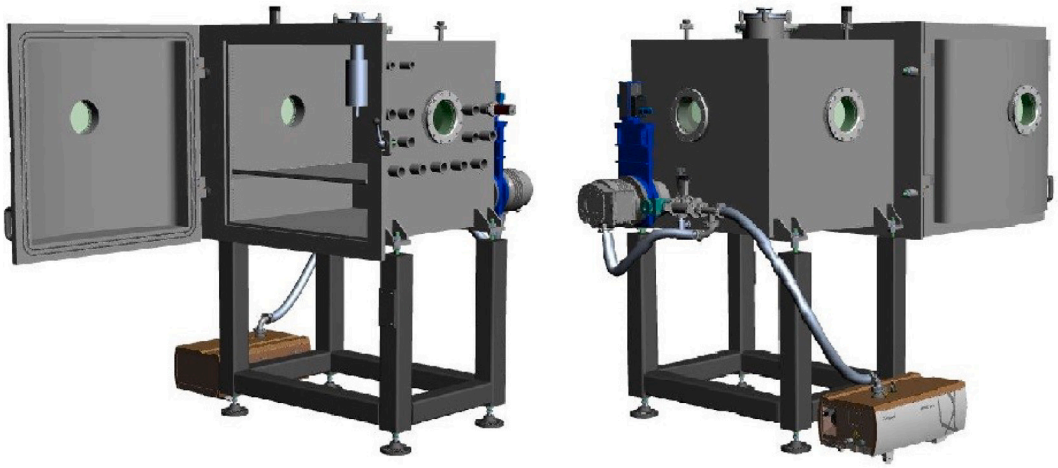

Fig. 1. 3D model of PISCES viewed from the front (left) and the back (right).

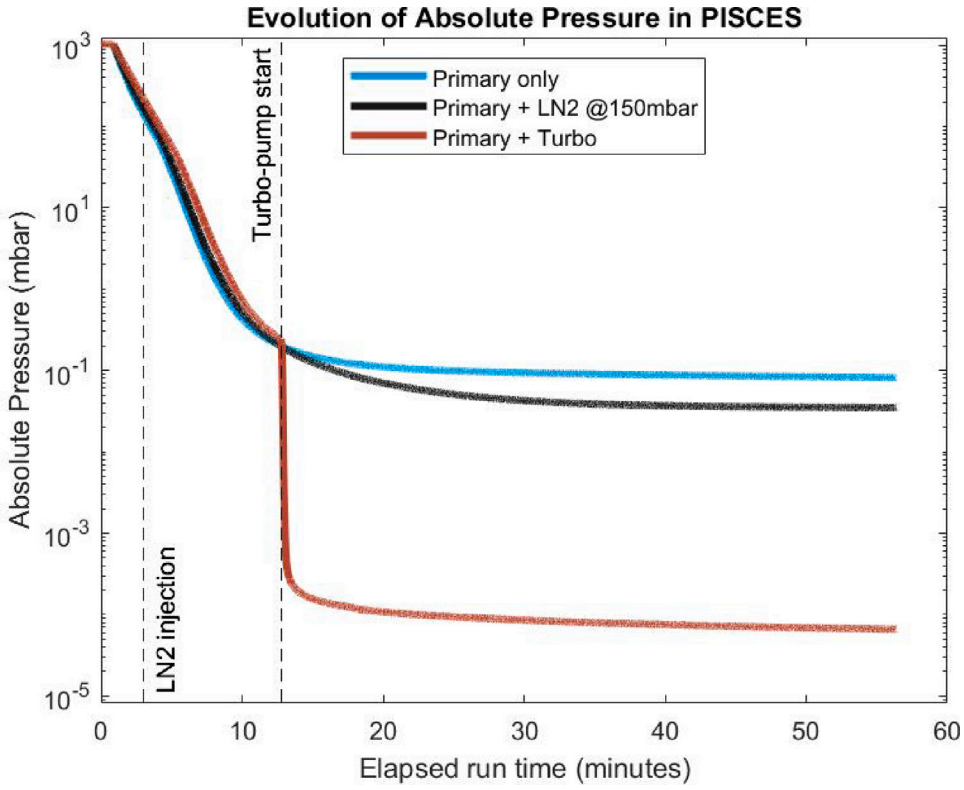

Fig. 2. Various operating modes of PISCES using combination of cryo-pumping with primary and/or turbo-pump.

- One multi-pin electrical feedthrough (41 connectors) for power delivery mounted on a DN50 KF flange (using adapters for DN40 KF port).
- Three custom-made differential pressure sensor line feedthroughs (12 lines each), using Swagelok Ultra-Torr vacuum fittings.
- Two type K thermocouple feedthroughs (5 pairs each).
- Two gas inlet/outlet feedthroughs with 2 ×1/4-inch VCR line fittings.
- Two liquid nitrogen (LN_2) supply feedthroughs with 1/4-inch line fittings.
- Four 9-pin D-Sub standard connector feedthroughs are used to interface with the vacuum-compatible motorised 3-axis linear translation stage.

2.1.2. Thermal control

Although PISCES does not feature controlled wall-cooling for true environmental temperature control, the temperature of an experimental setup inside PISCES can be lowered to cryogenic levels using the LN_2 feedthroughs. By circulating liquid nitrogen from an external dewar, the lower limit of the thermal range outlined in Table 1 can be met in any parts of an experimental setup placed inside PISCES.

For experiments requiring smaller temperature gradients, where cryogenic cooling may be unsuitable, high-purity aluminium pellets, ranging in size from 3 mm to 10 mm are used as passive cooling media. These pellets can be pre-cooled in laboratory freezers to temperatures as low as ~200 K and then placed in direct contact with specific components of the experimental setup inside PISCES.

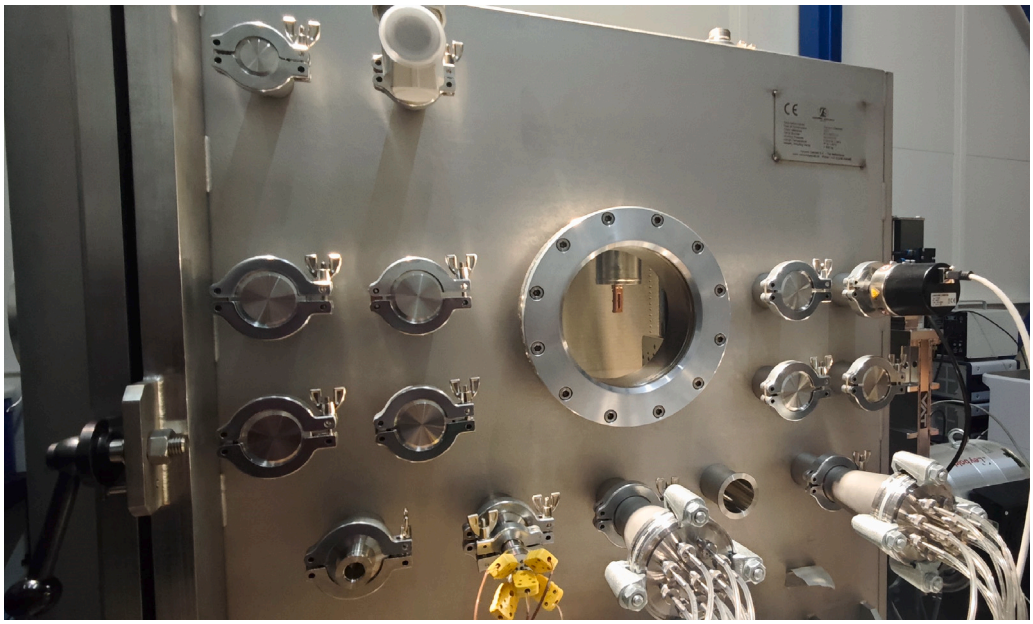

Fig. 3. Close-up view of the DN40 KF flanges for the feedthroughs on the side of the PISCES plateform.

Conversely, to increase the temperature inside PISCES, local additions of heat to the system are possible using several silicone heating foils with IPX7 rating from Thermo Technologies. There are connected to a Multicomp Pro MP711057 programmable Direct Current (DC) bench top power supply using the multi-pin feedthrough. With this arrangement, up to 300 W of electrical power can be supplied to the heating foils enabling precise temperature increases where required.

2.2. The sensors suite

Accurate sensors are key to understanding processes occurring during an experiment in PISCES. The two main parameters monitored for experiments are temperature and pressure at various locations in the chamber.

2.2.1. Temperature sensors

Type K thermocouples are placed at various locations to monitor temperature variations in PISCES. For surface-mounted applications, the thermocouples are secured using 3M 5413 polyimide film, while for flow temperature measurements (see Section 3.1), they are embedded in dedicated cavities within the experiment and sealed using melted Tecbond 7784 polyamide. These thermocouples operate with a nickel alloy junction (chromel: 90% nickel and 10% chromium, alumel: 95% nickel, 2% manganese, 2% aluminium and 1% silicon). They have an operational temperature range of approximately 80 K to 600 K.

The thermocouples are routed through the vacuum chamber via the dedicated feedthroughs and connected to an NI 9213 CompactDAQ temperature input module (see Appendix A).

2.2.2. Pressure sensors

The absolute vacuum pressure of the chamber is monitored by a set of three gauges:

- two THERMOVAC TTR 101 Transmitters (Leybold) with a monitored pressure range of 5.10^{-5} mbar to 1500 mbar. One is mounted directly on the chamber while the other is placed on the roots pump's line. The analogue output of these sensors is converted to absolute pressure readings through the following equation provided by the manufacturer:

$$P_{mbar} = 10^{\frac{V_{out}-6.143}{1.286}} \quad (1)$$

- one PENNINGVAC PTR 90 cold cathode transmitter (Leybold) which covers a measurement range of 5.10^{-9} mbar to 1000 mbar is also mounted on the chamber (see Fig. 3 on the top right).

$$P_{mbar} = 10^{1,667 \cdot V_{out} - 11.33} \quad (2)$$

To record minute pressure variations in experimental setups inside PISCES, we use a combination of two different piezoresistive sensors simultaneously to measure differential pressures. This ensures low uncertainties in the pressure measurements (see Appendix B for additional details). The AMS-6916-0010-D-H-DIL chip from AMSYS covers a differential pressure range of 10 mbar and the NPA-500B-05WG chip from Amphenol All/Advanced Sensors spans 12,5 mbar, which is sufficient to cover most practical modelling cases with PISCES. The sensors are housed outside the vacuum chamber in a dedicated temperature-stabilised casing, minimising environmental interference. Each sensor is powered by a 5 V supply, connected via DIN Rail distribution terminals to an NI 9201 CompactDAQ voltage input module. Data are converted from voltage to differential pressure by virtue of the sensors' ratio-metric output design using Eq. (3).

$$P_{mbar} = P_{max-mbar} \frac{V_{out} - 0.1 \cdot V_{supply}}{0.8 \cdot V_{supply}} \quad (3)$$

V_{out} is the measured analogue signal from the sensor, V_{supply} is the 5 V tension powering the sensor and P_{max} is the maximum differential pressure the sensor can record, 10 or 12.5 mbar depending on the chip.

A Raspberry Pi 4B within the casing monitors internal temperature and pressure using a Parallax Inc MS5607 chip sensor (see Appendix B for details on data correction and error propagation). The differential pressure sensors are connected to the model inside PISCES using Tygon 2375 and Versilon C-210-A polyolefin flexible tubing, which runs through the dedicated feedthroughs (see Section 2.1.1). The Tygon 2375 series has a closely related variant, Tygon 2475, which has been referenced in the NASA outgassing database from its 2011 formulation[3] as suitable for space applications, with a Total Mass Loss in % (TML%) of 0.26. While the manufacturer does not conduct outgassing rate tests on these updated formulation of the NASA-tested product specifically (internal communication), tests run in PISCES under vacuum conditions

[3] https://outgassing.nasa.gov/ accessed July 26, 2024

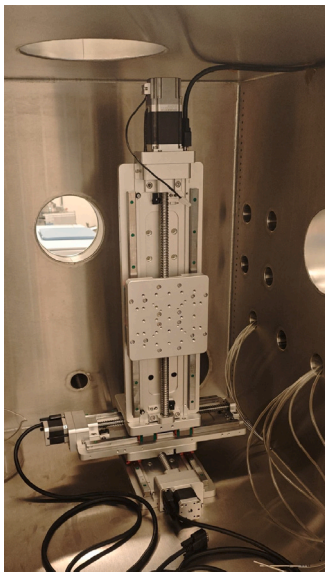

Fig. 4. Customised 3-axis motorised translation stages inside of PISCES.

result in a TML% lower than 0.1% for both formulation, confirming them as suitable to operate in the experimental setup.

2.3. Remote sample positioning system

PISCES will be integrated with several optical measurement solutions. The current design philosophy prioritises optical alignment using the portholes of PISCES prior to experiments. Experimental setups inside PISCES can be mounted on the customised 3-axis motorised translation stage (see Fig. 4). With this approach, various components of the experimental setup can be brought into focus from within the chamber, eliminating the need for systematic adjustments to external optical components during experiments.

This system, manufactured by Optics Focus,[4] tested in PISCES at pressures down to 10^{-5} mbar, allows movement along the XYZ axes with high precision:

- Z-axis (vertical movement): A CMOX-06-300-B-V motorised translation stage with a 300 mm travel range, 3.125 μm resolution, and a 30 kg load capacity. It includes a power-off brake for security.
- XY-plane (horizontal movement): Two CMOX-06-150-V high-precision motorised linear stages, each with a 150 mm travel range, 1.5625 μm resolution, and a 30 kg load capacity.
- Control system: All three stages are managed by an MOC-02-3-220 motion controller for NEMA23 stepper motors, supporting 1/2, 1/4, and 1/8 micro-step configurations for fine positional adjustments.

This customised translation stage utilises DB9 connections (see Section 2.1.1) to communicate between the controller and motorised stages. A standard RS232 interface allows direct control of stage positioning.

3. Examples of usage for PISCES

Hereafter one of the main research topic of PISCES, origins and dynamics of plumes of icy moons, is detailed. Using PISCES as an environmental chamber with pressure and temperature conditions matching those of icy moons, we study the relationship between subsurface terrain features like crevasse width, length, shape, temperature, rugosity and their effects on some plume characteristics such as mass fraction of icy particles to gas, particle size and distribution, particle and flow velocities.

3.1. Flagship experiment: Crevasse Laboratory Analogue for Moons — CLAM

3.1.1. Experimental protocol

The Crevasse Laboratory Analogue for Moons (CLAM) experimental setup is designed to replicate icy plumes within a controlled laboratory environment. It incorporates the following key elements to allow plume formation: liquid water connected to vacuum through a narrow crevasse.

- The subsurface liquid water reservoir is a cylindrical chamber with an inner diameter of 175 mm, sealed at the bottom, annotated 1 in Fig. 5.
- The crevasse analogue — representing the channel connecting the subsurface ocean to the icy moon's surface — is mounted on the reservoir lid using nitrile O-rings to ensure an airtight seal (annotated 3 in Fig. 5). Various geometries can be explored. Each design is created using the FreeCAD parametric modeller and fabricated in white V4 resin via a Form 3L 3D resin printer from Formlabs.
- The outer layer of the 3D-printed channel (noted 4 in Fig. 5) is used to cool the crevasse analogue to different temperatures, while the water reservoir is heated to maintain appropriate conditions depending on the hypothesis under investigation (see Section 2.1.2).
- Sensor ports (noted 5 and 6 on Fig. 5, also see Section 2.2) are connected to the appropriate interfaces (Section 2.1.1) at key locations within the channel (5 mm, 60 mm, 140 mm and 240 mm from the channel's inlet), enabling the recording of static pressure and temperature of the flow. These measurements are taken while the CLAM is placed inside PISCES, and the chamber pressure is lowered to simulate icy moons' environments.

A view of a CLAM setup connected to PISCES following an experimental run is shown in Fig. 6. The thermocouples (see Section 2.2.1) and differential pressure lines (see Section 2.2.2) are visible, connected to the feedthroughs described in Section 2.1.1, located on the right side of the figure.

For this experiment, aluminium pellets were pre-cooled to 215 K (as outlined in Section 2.1.2) and poured around the inner 7.5 mm channel, marked as (3) in Fig. 5. In the top left of the image, the bottom end of the cold finger is still partially covered in residual ice, formed from condensed vapour released during the experiment and not fully removed by the pumping system.

Fig. 7(a) presents the temperature readings obtained from testing a CLAM experiment within PISCES and 7(b) presents the pressure readings . Additionally, the integration of a Pitot probe (Kimo/Sauermann TPL-03-200-T model) at the vent location enables the measurement of gas flow velocity. These results correspond to an experiment conducted on a straight, vertically walled crevasse cooled to 215 K.

4. Conclusion and prospects

The Plumes and Ices Simulation Chamber for Enceladus and other moonS, PISCES for short, is the latest addition to the expanding family of experimental rigs used for planetary sciences. Developed at the Faculty of Aerospace Engineering at Delft University of Technology, PISCES has been designed and is used to support the Planetary Exploration group in advancing research on icy moons. With its innovative blend of dimensions, vacuum capabilities, thermal management and extensive sensor integration, PISCES is uniquely capable of providing a laboratory controlled environment to study large-scale processes observed on icy moons.

[4] https://optics-focus.com/ last accessed April 8, 2025

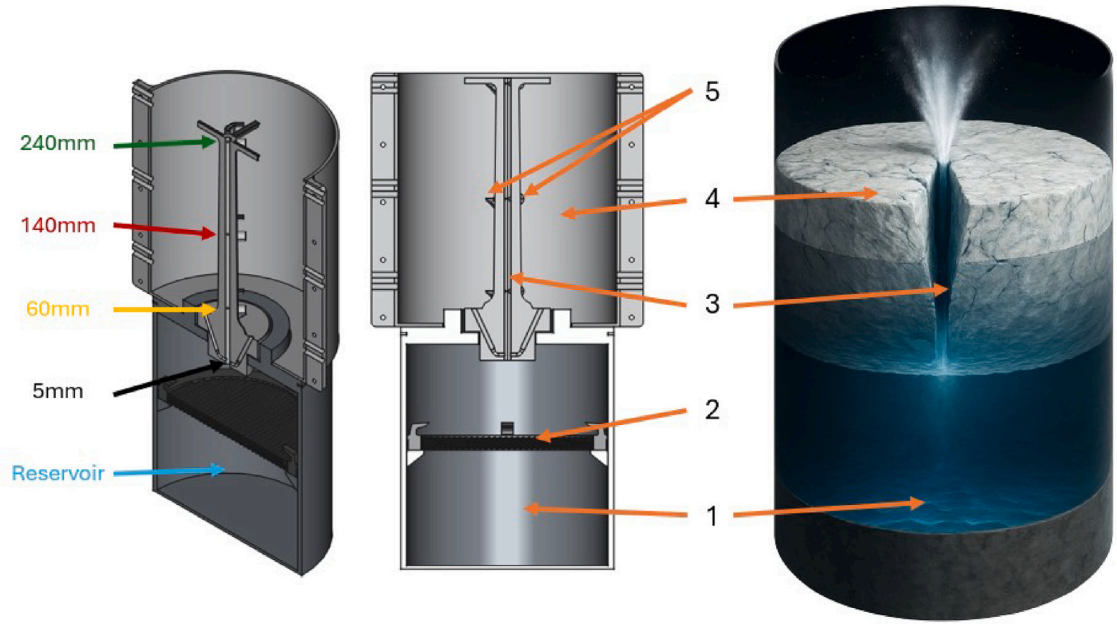

Fig. 5. 3D model of a CLAM on the left and middle, with the reservoir (1), a splash-screen (2), the channel (3) with holes integrated for thermocouples and pressure sensors (5), and the outer shell (4). On the right is an AI-generated rendition of the analogue for better understanding. The coloured legend on the left indicates the location of the sensors matching the temperature and pressure profiles given in Fig. 7(b).

Fig. 6. Photo of a CLAM setup cooled with aluminium pellet to 215 K and hooked to PISCES.

As we show in this article, PISCES is currently capable of producing pressure (down to 3×10^{-5} mbar) and temperature (down to 80 K) matching conditions found on icy moons of the Solar System. The CLAM experimental setup takes advantage of those environmental conditions inside PISCES to help investigate the relationship between sub-surface terrain properties and plume parameters.

In addition to the flagship CLAM experiments, PISCES is planned to be adapted for a variety of experimental setups, expanding its role in the study of icy moons.

To investigate surface properties of ices and analyse their composition, PISCES will operate in synergy with a Fourier Transform Infrared (FT-IR) spectrometer platform, specifically the Invenio system from Bruker.[5]

Depending on the experiment, transmittance and reflectance measurements will be conducted through PISCES' wide portholes, with the translation stages ensuring precise alignment between the sample matrix and the external optical measuring apparatus.

With this addition, PISCES would enable the study of ice surface properties under icy moon analogous conditions. These elements are critical considerations in the design of upcoming space missions targeting icy moons with lander concepts (Harmon et al., 2023). Research can also extend into materials science, particularly the study of space weathering of materials exposed to plume activity.

These research directions are part of ongoing projects, and their results will be documented in future publications.

As interest in icy celestial bodies continues to grow, driven by large-class missions, both current and future, PISCES is poised to become an essential tool for optimising mission planning, selecting and testing scientific instruments, and maximising the scientific return from upcoming explorations.

[5] https://www.bruker.com/en/products-and-solutions/infrared-and-raman/ft-ir-research-spectrometers/invenio-ft-ir-spectrometer.html last accessed April 23, 2025

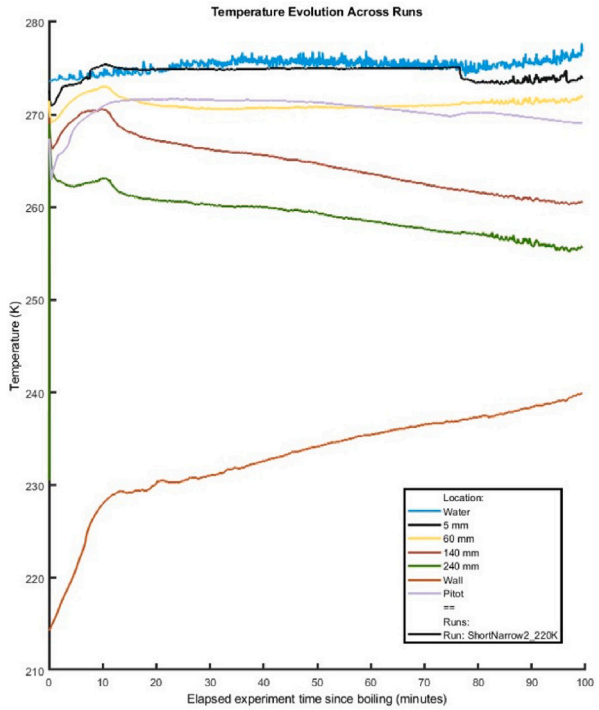

(a) Temperature evolution

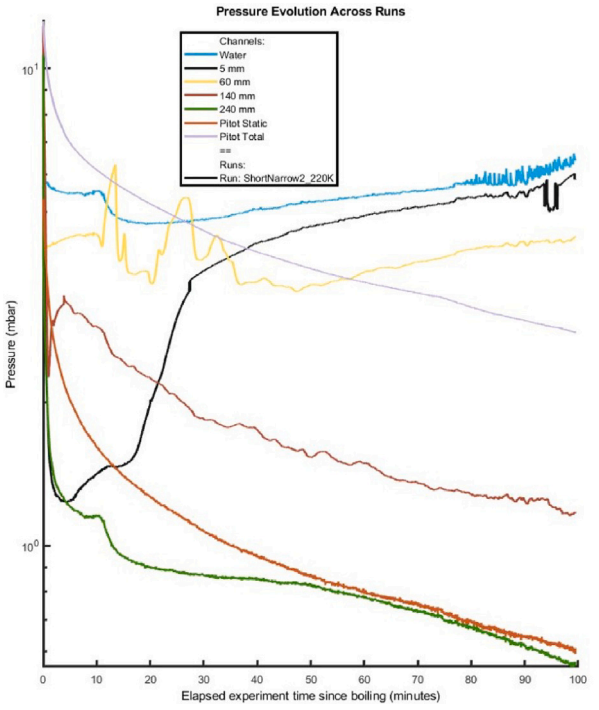

(b) Pressure evolution

Fig. 7. Temperature (a) and Pressure (b) evolution at the vent (240 mm), inside the channel (140 mm and 60 mm), at the inlet (5 mm) and in the reservoir. Distance in mm is given from the bottom of the 3D printed channel.

CRediT authorship contribution statement

Yaël R.A. Bourgeois: Writing – original draft, Methodology, Investigation. **Stéphanie M. Cazaux:** Writing – review & editing, Supervision, Project administration.

Declaration of competing interest

The authors declare that they have no known competing financial interests or personal relationships that could have appeared to influence the work reported in this paper.

Acknowledgements

The authors would like to thank the NWO PEPSci-II funding scheme for supporting their research on icy moons. We would also like to thank Dr. Ir. B. Root for the financing of the very first version of the CLAM setup.

Appendix A. Data acquisition

The analogue data coming from the thermocouples are routed through a 16-channel NI 9213 CompactDAQ temperature input module. Meanwhile, the analogue voltage output of the absolute and differential pressure sensors is routed to the workstation acquisition card through three National Instruments (NI) 9201 CompactDAQ voltage input module with 8 channels each. All data are sampled at 100 Hz and, for the pressures, transformed from volts into absolute and differential pressure values in a custom LabVIEW virtual instrument program using Eqs. (1)–(3).

The processed data are subsequently averaged every second and logged in a text file. Given the dynamics of the processes studied, this difference between sampling rate and logging rate allows for reasonable file size for hours-long experiments while still capturing transient fluctuations of the plume.

Appendix B. Differential pressure sensors' precision and calibration

Recent breakthroughs in Micro Electro-Mechanical Systems (MEMS) have opened up new avenues for small form factor sensors with great accuracy and robustness. In the area of differential pressure sensors, various types of sensing technology can be employed:

- capacitive sensors: a diaphragm is attached to one of the capacitor plates of the circuit. The pressure variations cause the diaphragm to move, changing the distance between the two plates and resulting in variations in electrical capacitance in the circuit, affecting the voltage output from the sensor.
- piezoresistive strain gauge sensors: a diaphragm is attached to one of the resistors of a Wheatstone bridge circuit. Small changes in the electrical resistance of the circuit caused by the movement of the diaphragm is converted to output voltage variations.
- thermal flow-through sensors: the flow caused by the difference in pressure between the two ports of the sensor travels across a heated section in the sensor. Two temperature sensors gauge this heat flow rate and with careful calibration, infer the difference in pressure to which the sensor is exposed to.

While very promising in accuracy and robustness, the flow-through technology sensors are not suited for PISCES' environmental conditions. The sensors detailed in 2.2.2 are piezoresistive strain gauge sensors.

B.1. Range and precision

As mentioned in Section Section 2.2.2, the AMS-6916-0010-D-H-DIL sensor has a gauge pressure difference between the two ports of the sensor that spans 0.15 *psi* or ~10.34 mbar while the NPA-500B-05WG sensor has a range of 5" of H_2O or ~12.45 mbar.

As per the manufacturer's data for both sensors, they have a maximum total error band of 1.5% of their Full Scale Output (FSO). This refers to the algebraic difference between the output signal measured at the maximum (P_{max}) and minimum (P_{min}) limits of the pressure range.

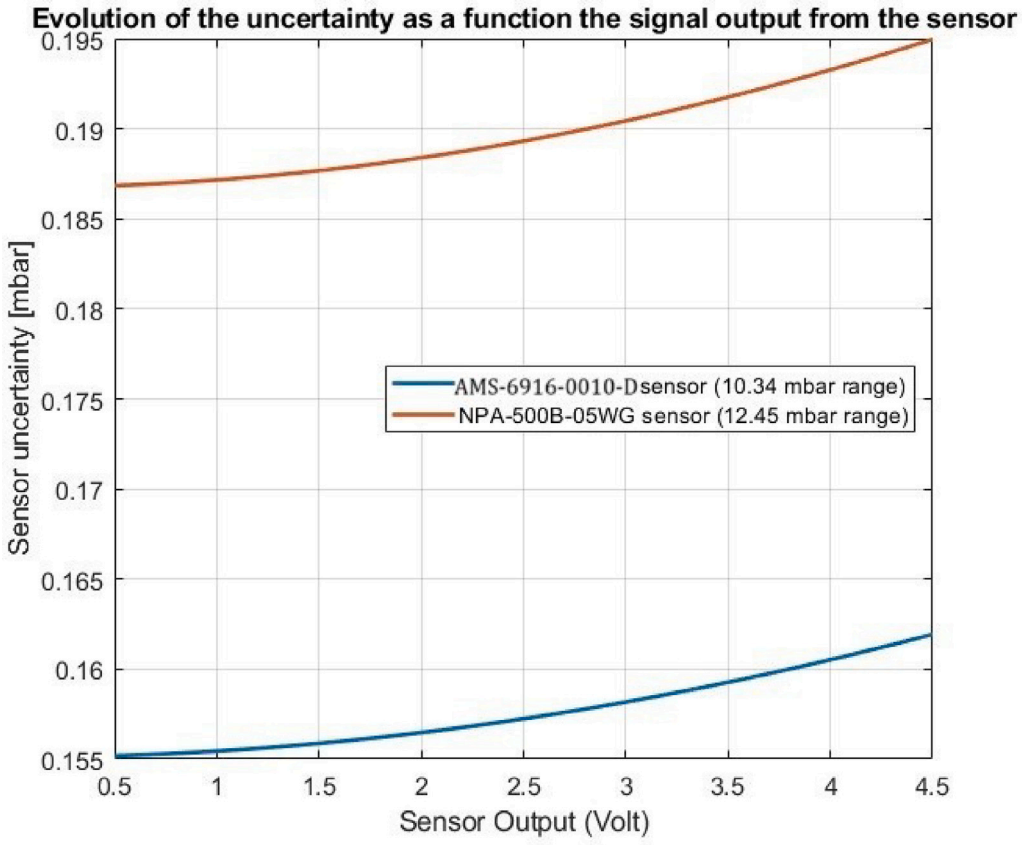

Fig. 8. Uncertainty in pressure measurement as a function of the sensors' output.

B.2. Calibration and correction

To account for "zero-offset" fluctuations, the sensors are initialised a few minutes prior to the start of the pumps in PISCES, and the P_{min} output (0 pressure difference between both ports) signal values are recorded. The values are *a posteriori* subtracted from the sensors' output during the experiment to recover the correct differential pressure readings.

As the voltage output of the differential pressure sensors is ratiometric to the supplied voltage following Eq. (3), the output of the 5 V power supply is also logged throughout any experiments to allow the possibility to correct any fluctuations, spikes or drops in the supplied voltage from the sensors output.

B.3. Error propagation

For each sensor, we will compute the error on the measured pressure using the propagated uncertainty equation :

$$(\sigma_P)^2 = \left(\frac{\partial P_{\text{mbar}}}{\partial V_{\text{out}}}\right)^2 (\sigma_{V_{\text{out}}})^2 + \left(\frac{\partial P_{\text{mbar}}}{\partial V_{\text{supply}}}\right)^2 (\sigma_{V_{\text{supply}}})^2 \tag{4}$$

Substituting with Eq. (3) yields the following partial derivatives:

$$\frac{\partial P_{\text{mbar}}}{\partial V_{\text{out}}} = \frac{P_{\text{max}}}{0.8 \cdot V_{\text{supply}}} \tag{5}$$

and

$$\frac{\partial P_{\text{mbar}}}{\partial V_{\text{supply}}} = \frac{-1.25 \cdot P_{\text{max}} \cdot V_{\text{out}}}{(V_{\text{supply}})^2} \tag{6}$$

With the knowledge of the total error band of the sensors from the manufacturer's data and the measured standard deviation of the 5 V power supply, we can then estimate the uncertainty σ_P as a function of V_{out} for each sensors, as reported on Fig. 8.

Since the sensors are meant to be combined and averaged per location, the resulting uncertainty for this combination is reflected in Eq. (7):

$$(\sigma_{P_{combined}})^2 = \left(\frac{\sigma_{BPS}}{2}\right)^2 + \left(\frac{\sigma_{NPA}}{2}\right)^2 \tag{7}$$

Finally, the total uncertainty will the quadratic combination of the statistical uncertainty determined from repeating the same experiments N times and the sensors' uncertainty σ_P as summarised with Eq. (8):

$$(\sigma_{P_{Total}})^2 = \left(\frac{\sigma_{exp}}{N}\right)^2 + (\sigma_{P_{combined}})^2 \tag{8}$$

Data availability

Data will be made available on request.

References

Brown, R.H., Clark, R.N., Buratti, B.J., Cruikshank, D.P., Barnes, J.W., Mastrapa, R.M., Bauer, J., Newman, S., Momary, T., Baines, K.H., Bellucci, G., Capaccioni, F., Cerroni, P., Combes, M., Coradini, A., Drossart, P., Formisano, V., Jaumann, R., Langavin, Y., Matson, D.L., McCord, T.B., Nelson, R.M., Nicholson, P.D., Sicardy, B., Sotin, C., 2006. Composition and physical properties of Enceladus' surface. Science 311 (5766), 1425–1428. http://dx.doi.org/10.1126/science.1121031.

Brown, M.E., Hand, K.P., 2013. Salts and radiation products on the surface of Europa. Astron. J. 145 (4), http://dx.doi.org/10.1088/0004-6256/145/4/110.

Bründl, T.-M., Linnartz, H., Cazaux, S., Chuang, K.-J., 2022. Laboratory studies of irradiated enceladus ice analogues. http://dx.doi.org/10.5194/epsc2022-877.

Chi, I., Gerges, D., Balcerski, J., 2024. GEER (Glenn extreme environments rig): Current project status. URL https://www1.grc.nasa.gov/space/geer/.

Choblet, G., Tobie, G., Buch, A., Čadek, O., Barge, L.M., Bēhounková, M., Camprubi, E., Freissinet, C., Hedman, M., Jones, G., Lainey, V., Gall, A.L., Lucchetti, A., MacKenzie, S., Mitri, G., Neveu, M., Nimmo, F., Olsson-Francis, K., Panning, M., Postberg, F., Saur, J., Schmidt, J., Sekine, Y., Shibuya, T., Sotin, C., Soucek, O.,

Szopa, C., Usui, T., Vance, S., Hoolst, T.V., 2022. Enceladus as a potential oasis for life: Science goals and investigations for future explorations. Exp. Astron. 54, 809–847. http://dx.doi.org/10.1007/s10686-021-09808-7.

Cruikshank, D.P., Roush, T.L., Owen, T.C., Geballe, T.R., De Bergh, C., Schmitt, B., Brown, R.H., Bartholomew, M.J., 1993. Ices on the surface of Triton. Science 261 (5122), 742–745. http://dx.doi.org/10.1126/SCIENCE.261.5122.742.

Dong, Y., Hill, T.W., Teolis, B.D., Magee, B.A., Waite, J.H., 2011. The water vapor plumes of Enceladus. J. Geophys. Res.: Space Phys. 116 (A10), http://dx.doi.org/10.1029/2011ja016693.

Fox-Powell, M., Slade, D., Siggs, D., Olsson-Francis, K., 2022. Experimentally probing the origin of Enceladus' plume: bubble-bursting and aerosol formation at the liquid/vapour interface. http://dx.doi.org/10.5194/epsc2022-1231.

Gao, P., Kopparla, P., Zhang, X., Ingersoll, A.P., 2016. Aggregate particles in the plumes of Enceladus. Icarus 264, 227–238. http://dx.doi.org/10.1016/j.icarus.2015.09.030.

Hamp, R., Olsson-Francis, K., Schwenzer, S., Pearson, V., 2024. An inorganic silicate simulant to represent the interior of Enceladus. Planet. Space Sci. 248, 105934. http://dx.doi.org/10.1016/j.pss.2024.105934.

Hansen, C.J., Esposito, L., Stewart, A.I.F., Colwell, J., Hendrix, A., Pryor, W., Shemansky, D., West, R., 2006. Enceladus' water vapor plume. Science 311 (5766), 1422–1425. http://dx.doi.org/10.1126/science.1121254.

Hansen, C.J., Esposito, L.W., Stewart, A.I.F., Meinke, B., Wallis, B., Colwell, J.E., Hendrix, A.R., Larsen, K., Pryor, W., Tian, F., 2008. Water vapour jets inside the plume of gas leaving Enceladus. Nature 456 (7221), 477–479. http://dx.doi.org/10.1038/nature07542.

Hansen, C.J., Shemansky, D.E., Esposito, L.W., Stewart, A.I.F., Lewis, B.R., Colwell, J.E., Hendrix, A.R., West, R.A., Waite, J.H., Teolis, B., Magee, B.A., 2011. The composition and structure of the Enceladus plume. Geophys. Res. Lett. 38 (11), http://dx.doi.org/10.1029/2011gl047415.

Harmon, J.M., Cable, M.L., Moreland, S.J., Andrade, J.E., 2023. Predicting the effect of surface properties on Enceladus for landing. Planet. Sci. J. 4, 150. http://dx.doi.org/10.3847/PSJ/acec49, URL https://iopscience.iop.org/article/10.3847/PSJ/acec49.

Iess, L., Stevenson, D.J., Parisi, M., Hemingway, D., Jacobson, R.A., Lunine, J.I., Nimmo, F., Armstrong, J.W., Asmar, S.W., Ducci, M., Tortora, P., 2014. The gravity field and interior structure of Enceladus. Science 344, 78–80. http://dx.doi.org/10.1126/science.1250551.

Ingersoll, A.P., Ewald, S.P., 2011. Total particulate mass in Enceladus plumes and mass of Saturn's E ring inferred from Cassini ISS images. Icarus 216 (2), 492–506. http://dx.doi.org/10.1016/j.icarus.2011.09.018.

Ingersoll, A.P., Nakajima, M., 2016. Controlled boiling on Enceladus. 2. Model of the liquid-filled cracks. Icarus 272, 319–326. http://dx.doi.org/10.1016/j.icarus.2015.12.040.

Ingersoll, A.P., Pankine, A.A., 2010. Subsurface heat transfer on Enceladus: Conditions under which melting occurs. Icarus 206 (2), 594–607. http://dx.doi.org/10.1016/j.icarus.2009.09.015.

Jensen, L.L., Merrison, J., Hansen, A.A., Mikkelsen, K.A., Kristoffersen, T., Nørnberg, P., Lomstein, B.A., Finster, K., 2008. A facility for long-term mars simulation experiments: The mars environmental simulation chamber (MESCH). Astrobiology 8, 537–548. http://dx.doi.org/10.1089/ast.2006.0092.

Khurana, K.K., Kivelson, M.G., Stevenson, D.J., Schubert, G., Russell, C.T., Walker, R.J., Polanskey, C., 1998. Induced magnetic fields as evidence for subsurface oceans in Europa and Callisto. Nature 395, 777–780. http://dx.doi.org/10.1038/27394.

Kieffer, S.W., Lu, X., McFarquhar, G., Wohletz, K.H., 2009. A redetermination of the ice/vapor ratio of Enceladus' plumes: Implications for sublimation and the lack of a liquid water reservoir. Icarus 203 (1), 238–241. http://dx.doi.org/10.1016/j.icarus.2009.05.011.

Kipfer, K.A., Galli, A., Riedo, A., Tulej, M., Wurz, P., Ligterink, N.F., 2024. Complex ice chemistry: A comparative study of electron irradiated planetary ice analogues containing methane. Icarus 410, 115742. http://dx.doi.org/10.1016/j.icarus.2023.115742.

Kite, E.S., Rubin, A.M., 2016. Sustained eruptions on Enceladus explained by turbulent dissipation in tiger stripes. Proc. Natl. Acad. Sci. 113 (15), 3972–3975. http://dx.doi.org/10.1073/pnas.1520507113.

Lainey, V., Rambaux, N., Tobie, G., Cooper, N., Zhang, Q., Noyelles, B., Baillié, K., 2024. A recently formed ocean inside Saturn's moon Mimas. Nature 626, 280–282. http://dx.doi.org/10.1038/s41586-023-06975-9.

Lellouch, E., De Bergh, C., Sicardy, B., Ferron, S., Käufl, H.U., 2010. Detection of CO in Triton's atmosphere and the nature of surface-atmosphere interactions. Astron. Astrophys. 512 (12), L8. http://dx.doi.org/10.1051/0004-6361/201014339, URL https://www.aanda.org/articles/aa/abs/2010/04/aa14339-10/aa14339-10.html.

Ligier, N., Paranicas, C., Carter, J., Poulet, F., Calvin, W.M., Nordheim, T.A., Snodgrass, C., Ferellec, L., 2019. Surface composition and properties of Ganymede: Updates from ground-based observations with the near-infrared imaging spectrometer SINFONI/VLT/ESO. Icarus 333, 496–515. http://dx.doi.org/10.1016/J.ICARUS.2019.06.013.

Ligier, N., Poulet, F., Carter, J., Brunetto, R., Gourgeot, F., 2016. VLT/SINFONI OBservations of Europa: new insights into the surface composition. Astron. J. 151 (6), 163. http://dx.doi.org/10.3847/0004-6256/151/6/163.

Mateo-Marti, E., 2014. Planetary atmosphere and surfaces chamber (PASC): A platform to address various challenges in astrobiology. Challenges 5, 213–223. http://dx.doi.org/10.3390/challe5020213.

Matson, D.L., Castillo-Rogez, J.C., Davies, A.G., Johnson, T.V., 2012. Enceladus: A hypothesis for bringing both heat and chemicals to the surface. Icarus 221 (1), 53–62. http://dx.doi.org/10.1016/j.icarus.2012.05.031.

Mitchell, K.L., Rabinovitch, J., Scamardella, J.C., Cable, M.L., 2024. A proposed model for cryovolcanic activity on Enceladus driven by volatile exsolution. J. Geophys. Res.: Planets 129, http://dx.doi.org/10.1029/2023JE007977.

Muñoz Caro, G.M., Meierhenrich, U.J., Schutte, W.A., Barbier, B., Segovia, A.A., Rosenbauer, H., Thiemann, W.H.-P., Brack, A., Greenberg, J.M., 2002. Amino acids from ultraviolet irradiation of interstellar ice analogues. Nature 416, 403–406. http://dx.doi.org/10.1038/416403a.

Nakajima, M., Ingersoll, A.P., 2016. Controlled boiling on Enceladus. 1. Model of the vapor-driven jets. Icarus 272, 309–318. http://dx.doi.org/10.1016/j.icarus.2016.02.027.

Nimmo, F., Pappalardo, R.T., 2016. Ocean worlds in the outer solar system. J. Geophys. Res.: Planets 121, 1378–1399. http://dx.doi.org/10.1002/2016JE005081.

Perry, M., Teolis, B., Hurley, D., Magee, B., Waite, J., Brockwell, T., Perryman, R., McNutt, R., 2015. Cassini INMS measurements of Enceladus plume density. Icarus 257, 139–162. http://dx.doi.org/10.1016/j.icarus.2015.04.037.

Porco, C.C., Helfenstein, P., Thomas, P.C., Ingersoll, A.P., Wisdom, J., West, R., Neukum, G., Denk, T., Wagner, R., Roatsch, T., Kieffer, S., Turtle, E., McEwen, A., Johnson, T.V., Rathbun, J., Veverka, J., Wilson, D., Perry, J., Spitale, J., Brahic, A., Burns, J.A., DelGenio, A.D., Dones, L., Murray, C.D., Squyres, S., 2006. Cassini observes the active south pole of Enceladus. Science 311 (5766), 1393–1401. http://dx.doi.org/10.1126/science.1123013.

Portyankina, G., Esposito, L.W., Aye, K.-M., Hansen, C.J., Ali, A., 2022. Modeling the complete set of Cassini's UVIS occultation observations of Enceladus' plume. Icarus 383, 114918. http://dx.doi.org/10.1016/j.icarus.2022.114918.

Postberg, F., 2014. The latest on hydrothermal activity on Enceladus from Cassini and laboratory work. Science 344, 1092–1093.

Postberg, F., Kempf, S., Schmidt, J., Brilliantov, N., Beinsen, A., Abel, B., Buck, U., Srama, R., 2009. Sodium salts in E-ring ice grains from an ocean below the surface of Enceladus. Nature 459, 1098–1101. http://dx.doi.org/10.1038/nature08046.

Quirico, E., Douté, S., Schmitt, B., De Bergh, C., Cruikshank, D.P., Owen, T.C., Geballe, T.R., Roush, T.L., 1999. Composition, Physical State, and Distribution of Ices at the Surface of Triton. Icarus 139 (2), 159–178. http://dx.doi.org/10.1006/ICAR.1999.6111.

Schmidt, J., Brilliantov, N., Spahn, F., Kempf, S., 2008. Slow dust in Enceladus' plume from condensation and wall collisions in tiger stripe fractures. Nature 451, 685–688. http://dx.doi.org/10.1038/nature06491.

Sekine, Y., Shibuya, T., Postberg, F., Hsu, H.-W., Suzuki, K., Masaki, Y., Kuwatani, T., Mori, M., Hong, P.K., Yoshizaki, M., Tachibana, S., iti Sirono, S., 2015. High-temperature water–rock interactions and hydrothermal environments in the chondrite-like core of Enceladus. Nat. Commun. 6, 8604. http://dx.doi.org/10.1038/ncomms9604.

Sobrado, J.M., Martín-Soler, J., Martín-Gago, J.A., 2014. Mimicking Mars: A vacuum simulation chamber for testing environmental instrumentation for Mars exploration. Rev. Sci. Instrum. 85, http://dx.doi.org/10.1063/1.4868592.

Spencer, J.R., Nimmo, F., 2013. Enceladus: An active ice world in the Saturn system. Annu. Rev. Earth Planet. Sci. 41, 693–717. http://dx.doi.org/10.1146/annurev-earth-050212-124025.

Spencer, J.R., Pearl, J.C., Segura, M., Flasar, F.M., Mamoutkine, A., Romani, P., Buratti, B.J., Hendrix, A.R., Spilker, L.J., Lopes, R.M.C., 2006. Cassini encounters Enceladus: Background and the discovery of a south polar hot spot. Science 311 (5766), 1401–1405. http://dx.doi.org/10.1126/science.1121661.

Steenstra, E.S., 2024. Probing Venus' enigmatic evolution with the new Venus simulation laboratory at TU delft. http://dx.doi.org/10.5194/epsc2024-388.

ten Kate, I.L., Reuver, M., 2016. PALLAS: Planetary analogues laboratory for light, atmosphere, and surface simulations. Geol. En Mijnbouw/Netherlands J. Geosci. 95, 183–189. http://dx.doi.org/10.1017/njg.2015.19.

Thomas, P., Tajeddine, R., Tiscareno, M., Burns, J., Joseph, J., Loredo, T., Helfenstein, P., Porco, C., 2016. Enceladus's measured physical libration requires a global subsurface ocean. Icarus 264, 37–47. http://dx.doi.org/10.1016/j.icarus.2015.08.037.

Tian, F., Stewart, A., Toon, O., Larsen, K., Esposito, L., 2007. Monte Carlo simulations of the water vapor plumes on Enceladus. Icarus 188 (1), 154–161. http://dx.doi.org/10.1016/j.icarus.2006.11.010.

Tucker, O.J., Combi, M.R., Tenishev, V.M., 2015. 2D models of gas flow and ice grain acceleration in Enceladus' vents using DSMC methods. Icarus 257, 362–376.

van der Hijden, N.J., Giordano, F., Scholts, S.O.O., Sklavenitis, S., Bründl, T.-M., Bourgeois, Y.R., Schrijer, F.F., Cazaux, S.M., 2024. Linking Enceladus' plume characteristics to the crevasse properties. Icarus 417, 116114.

Vance, S., Bouffard, M., Choukroun, M., Sotin, C., 2014. Ganymede's internal structure including thermodynamics of magnesium sulfate oceans in contact with ice. Planet. Space Sci. 96, 62–70. http://dx.doi.org/10.1016/j.pss.2014.03.011.

Yeoh, S.K., Chapman, T.A., Goldstein, D.B., Varghese, P.L., Trafton, L.M., 2015. On understanding the physics of the Enceladus south polar plume via numerical simulation. Icarus 253, 205–222. http://dx.doi.org/10.1016/j.icarus.2015.02.020.

Yeoh, S.K., Li, Z., Goldstein, D.B., Varghese, P.L., Levin, D.A., Trafton, L.M., 2017. Constraining the Enceladus plume using numerical simulation and Cassini data. Icarus 281, 357–378. http://dx.doi.org/10.1016/j.icarus.2016.08.028.